Research Square

Preprints are preliminary reports that have not undergone peer review.
They should not be considered conclusive, used to inform clinical practice,
or referenced by the media as validated information.

3D-Printed Sustainable PLA/Flax Sandwich Panels Featuring Antitrichiral Cores: Effects of Geometry Parameters, and Density on Mechanical Performance

Anis Hamrouni

anis_hamrouni@yahoo.com

Le Mans Université

Kamel Bousnina

ENSIT

Jean-Luc Rebiere

Le Mans Université

Abderrahim El-Mahi

Le Mans Université

Moez Beyaoui

École nationale d'Ingénieurs de Sfax

Mohamed Haddar

École nationale d'Ingénieurs de Sfax

Research Article

Keywords: Auxetic, Antitrichiral cores, 3D printing, Energy absorption, Compression, Indentation, composite, PLA/Flax, sandwich structure

Posted Date: September 9th, 2026

DOI: https://doi.org/10.21203/rs.3.rs-10718676/v1

License: This work is licensed under a Creative Commons Attribution 4.0 International License.
Read Full License

Additional Declarations: No competing interests reported.

3D-Printed Sustainable PLA/Flax Sandwich Panels Featuring Antitrichiral Cores: Effects of Geometry Parameters, and Density on Mechanical Performance

Anis Hamrouni[1,2*], Kamel Bousnina[3], Jean-Luc Rebiere[1], Abderrahim El-Mahi[1], Moez Beyaoui[2], Mohamed Haddar[2]

[1]Acoustic Laboratory of Le Mans University (LAUM) UMR CNRS 6613, Av. O. Messiaen, 72085, Le Mans cedex 9, France.
[2]Laboratory of Mechanics Modeling and Production (LA2MP), National School of Engineers of Sfax, University of
Sfax, Sfax, Tunisia
[3]National School of Engineering of Tunis, University of Tunis, LMPE Laboratory, Avenue Taha Hussein, Montfleury, 1008 Tunis, Tunisia.

*E-mail, anis_hamrouni@yahoo.com, (Corresponding author Anis Hamrouni).
Orcid: 0000-0001-7254-307X

Author contributions: Anis Hamrouni: Investigation, Writing - Original draft, Methodology, Software. Kamel Bousnina: Data Curation, Visualization. Jean-Luc Rebiere: Review & Editing. Abderrahim El Mahi: Review & Editing. Moez Beyaoui: Review & Editing. Mohamed Haddar: Supervisor.

Data availability: The proposed research does not use any datasets.

Statements and Declarations: The authors have no relevant financial or non-financial interests to disclose.
.

3D-Printed Sustainable PLA/Flax Sandwich Panels Featuring Antitrichiral Cores: Effects of Geometry Parameters, and Density on Mechanical Performance

Abstract:

This work investigates the quasi-static mechanical response and energy-absorption capability of 3D-printed sandwich panels featuring anti-trichiral PLA/flax cores. The architected metamaterial cores are fabricated by fused deposition modeling using a bio-based composite filament, and their geometry is systematically varied through node radius, ligament length, and number of unit cells across the width. A detailed CAD design is used to generate antitrichiral lattices with different core densities, which are then printed under controlled processing conditions. Compression and indentation tests are performed to characterize global stiffness, plateau stress, load displacement behavior, and dissipated energy, thereby assessing the influence of geometric parameters on structural performance. Results show that increasing node radius and core thickness, or decreasing ligament length, enhances stiffness and significantly improves energy absorption in both compression and indentation, with denser configurations exhibiting stable, progressive collapse suitable for protective applications. The combination of auxetic antitrichiral topology and sustainable PLA/flax composite enables lightweight, tunable, and environmentally friendly core designs. The findings provide quantitative guidelines for tailoring geometry performance relationships in anti-trichiral cores and highlight their potential for impact-mitigation and indentation-resistant sandwich structures in applications where both mechanical efficiency and sustainability are required.
.

Keywords: *Auxetic*, Antitrichiral cores, 3D printing, Energy absorption, Compression, Indentation, composite, PLA/Flax, sandwich structure.

1. Introduction

Energy-absorbing architected materials are designed to redistribute and dissipate mechanical loads through controlled deformation, thereby protecting critical components under service and accidental conditions [1,2]. Such structures have become increasingly important in engineering sectors where weight reduction, impact resistance, and structural reliability must be achieved simultaneously, including transportation, aerospace, civil engineering, and personal protection [3–7]. In many of these applications, the global response is not governed solely by the bulk properties of the constituent material but is strongly influenced by the topology, relative density, and hierarchical organization of the underlying architecture [8–10]. Within this framework, lattice and metamaterial cores have emerged as promising candidates for lightweight, high-performance energy-absorbing components in sandwich panels and protective systems.

Auxetic cellular materials, characterized by a negative Poisson's ratio, exhibit lateral expansion under tension and lateral contraction under compression, which can lead to enhanced indentation resistance, shear stiffness, and energy absorption compared with conventional honeycomb or foam cores at comparable mass [11–13]. Typical auxetic topologies include re-entrant honeycombs, rotating rigid-unit systems, and chiral or anti-chiral lattices, all of which derive their unusual behavior from geometry rather than from any exotic constituent material. Recent

reviews and experimental studies have shown that tuning parameters such as cell shape, ligament orientation, and connectivity allows significant control over stiffness, strength, and failure mechanisms in auxetic structures.

Among these configurations, chiral and anti-chiral lattices composed of circular nodes connected by tangential ligaments have attracted particular interest because they can achieve highly tunable in-plane mechanical properties and Poisson's ratios through relatively simple geometric modifications [14–17]. In-plane investigations of tri-chiral and anti-trichiral cellular structures have demonstrated that variations in node radius, ligament thickness, and cell aspect ratio markedly affect elastic stiffness, load-carrying capacity, and energy absorption, with optimized auxetic designs outperforming non-auxetic reference architectures [18–20]. Anti-trichiral lattices, in particular, can combine low relative density with large recoverable strains and stable plateau-type responses, making them attractive for crashworthiness, impact mitigation, and indentation-resistant sandwich cores [21,22].

The practical use of such complex auxetic geometries has been greatly facilitated by advances in additive manufacturing (AM), which enable the fabrication of intricate three-dimensional lattices that are difficult or impossible to produce using conventional techniques. Material-extrusion processes such as Fused Deposition Modeling (FDM) are especially suitable for polymeric lattices because they offer low cost, relatively simple operation, and substantial geometric freedom, allowing controlled variation of cell topology and relative density within a single part. Experimental studies on 3D-printed lattice cores have confirmed that AM can deliver high specific stiffness and energy absorption under compression, shear, and bending, indicating strong potential for sandwich structures in structural and protective applications.

In the specific context of chiral and anti-chiral lattices, additive manufacturing has enabled direct exploration of geometry property relationships, showing that their mechanical response is sensitive not only to ideal geometric parameters but also to process-induced features such as layer thickness, build orientation, and interlayer bonding quality. It has been reported that defects associated with printing, such as voids at nodes or imperfect fusion along ligaments, may significantly alter the auxetic response and reduce failure strain, highlighting the need to consider process structure property interactions when designing 3D-printed auxetic cores. Consequently, systematic experimental investigations that couple detailed geometric design of anti-trichiral lattices with realistic AM conditions are essential to establish robust design strategies.

Concurrently, rising environmental concerns are driving a transition from petroleum-based polymers toward bio-based and biodegradable alternatives such as polylactic acid (PLA) and natural-fiber-reinforced biocomposites [23–25]. PLA is a thermoplastic derived from renewable resources, offering good stiffness, relatively low processing temperature, and excellent compatibility with FDM-based 3D printing. When reinforced with flax fibers, PLA can exhibit substantially improved stiffness, strength, and damage tolerance, while maintaining a reduced environmental footprint compared with traditional glass- or carbon-fiber composites. Mechanical and processing studies on PLA/flax composites and related bio-based systems have demonstrated that appropriate fiber volume fraction, fiber architecture, and printing parameters can yield high-performance, recyclable or biodegradable structural components [25–27].

Recent work on 3D-printed PLA/flax and other flax-reinforced PLA systems has shown that these materials can achieve mechanical performance suitable for load-bearing and semi-structural applications, including sandwich skins, cores, and lattice-type reinforcements [28,29]. Continuous or short flax fiber reinforcement has been reported to enhance tensile and flexural properties, fatigue resistance, and energy absorption capability, thus enabling the design of sustainable lightweight structures with competitive specific properties [30,31]. However, the integration of such bio-based composites into architected auxetic cores particularly anti-trichiral geometries remains only partially explored, especially regarding their performance under compression and indentation relevant to protective sandwich panels.

While there is now a substantial body of research on auxetic materials and structures, including re-entrant honeycombs and chiral lattices, the literature on anti-trichiral cores manufactured from sustainable polymer composites is still limited. Many previous studies have been conducted using metallic alloys or neat polymers; however, few studies have been carried out on structures reinforced with natural fibers, leaving open questions on how the addition of flax fibers influences the stiffness, strength, and energy dissipation of auxetic cores. In particular, the combined effects of node radius, ligament length, and core density on the compression and indentation response of anti-trichiral PLA/flax sandwich panels have not yet been systematically quantified.

Moreover, although it is recognized that auxetic and anti-chiral lattices can provide tunable energy absorption and indentation resistance, comprehensive parametric studies that map the relationships between geometric parameters, relative density, and key performance indicators such as plateau stress, indentation stiffness, and dissipated energy remain scarce for bio-based composite systems. Such knowledge is crucial for establishing design guidelines that balance lightweight requirements, mechanical performance, and environmental impact, and for benchmarking anti-trichiral cores against more conventional solutions like honeycombs, foams, or non-auxetic lattices.

In this context, the present work focuses on 3D-printed sustainable sandwich panels incorporating anti-trichiral cores made from a PLA/flax composite filament specifically designed for FDM. The main objective is to elucidate how geometric parameters and core density govern the quasi-static mechanical behavior of these structures under compression and indentation loading. A family of anti-trichiral lattice cores is manufactured with systematically varied node radius, ligament length, and number of unit cells across the width, while maintaining consistent printing conditions and material system, in order to isolate topological effects on performance.
Through an experimental program, load-displacement and stress-strain responses are obtained and used to evaluate stiffness, plateau stress, and absorbed energy for different core configurations. By correlating these metrics with geometric parameters and relative density, the study aims to provide a deeper understanding of the design space of anti-trichiral PLA/flax cores and to demonstrate their potential as tunable, sustainable energy-absorbing elements for sandwich structures. The results are expected to support the development of performance-based design guidelines for auxetic cores in applications where both mechanical efficiency and environmental responsibility are critical design drivers.

2. Materials and Experimental Methods

2.1 FDM Process

The studied antitrichiral material consisted of a composite blend of polylactic acid reinforced with short flax fibers, exhibiting a 1000 $kg \cdot m^{-3}$ density, a Young's modulus of 3400 MPa, and a Poisson's ratio of 0.3. Flax fibers represented 20% of the total volume fraction. The PLA/flax composite filament, supplied by NANOVIA [32], had a diameter of 1.75 mm and was specifically designed for additive manufacturing due to its biodegradable, renewable, and recyclable nature, offering an eco-friendly alternative for engineering applications.
Metamaterial samples were fabricated using a RAISE3D Pro2Plus printer, a high-performance industrial 3D printer renowned for its precision and quality finishes. The composite filament was chosen for its mechanical robustness and long-term stability, qualities essential for this study. Prior to printing, printer calibration and validation were performed to optimize performance. Printing was conducted with critical parameters aligned to the filament manufacturer's guidelines: a nozzle diameter of 0.4 mm, nozzle temperature at 220°C tailored to the composite's melting range to ensure optimal layer bonding and material flow, and a platform temperature of 60°C to enhance first-layer adhesion. The print speed was set at 60 mm/s to balance dimensional accuracy with reasonable fabrication time. Finally, a layer thickness of 0.2 mm was employed to achieve a compromise between surface smoothness, impacting the mechanical integrity of the metamaterials, and overall print duration.

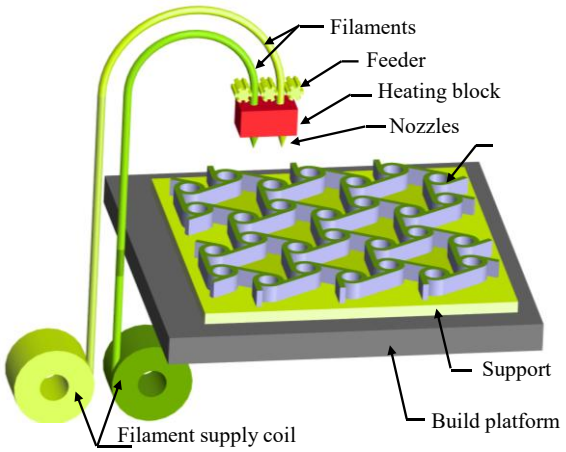


Figure 1. FDM Process.

A detailed CAD model of the metamaterial was created, incorporating key geometric parameters of its antitrichiral lattice. This CAD model was exported as an .stl file and imported into Idea Maker software, which converted it into G-Code instructions compatible with the RAISE3D Pro2Plus printer. The metamaterial was then fabricated by extruding the composite filament through a heated nozzle, building the structure layer by layer according to the programmed G-Code path (Figure 1). Throughout printing, critical parameters such as extrusion flow rate, layer thickness, and cooling rate were continuously monitored and adjusted to maintain optimal print quality. Upon completion, specimens were carefully detached from the build platform and subjected to necessary post-processing

steps, including cleaning and inspection [33]. The integration of precise CAD design, advanced 3D printing technology, and controlled manufacturing conditions enabled the production of metamaterials with accurately defined structural cell densities, tailored to the research objectives.

2.2 Antitrichiral structure

This study examines the mechanical behavior of 3D-printed anti-trichiral architected lattices made from a PLA matrix reinforced with short flax fibers (Figure 2). Experimental tests were designed to investigate the geometric parameters effect on the material's mechanical performance. Specimens were fabricated with varying cell dimensions according to their geometric parameters, as summarized in Table I. The relative core density was calculated using Equation 1. The unit cells are arranged within an equilateral triangular framework, where L denotes the ligament length determined from Equation 2, r is the radius of the cylindrical nodes, and t represents the cell wall thickness. The cell plane is defined in the X and Y directions, while the out-of-plane thickness corresponds to the Z direction. The periodic cell length along the Y direction is represented by H, and the specimen thickness is denoted by e. The parameters H and L were determined based on the number of cells across the specimen width (b), which was kept constant at 25 mm. Consequently, for specimens containing one cell across the width (1CW), L equals 4.16 mm; for two cells (2CW), L equals 2.08 mm; and for three cells (3CW), L equals 1.38 mm.

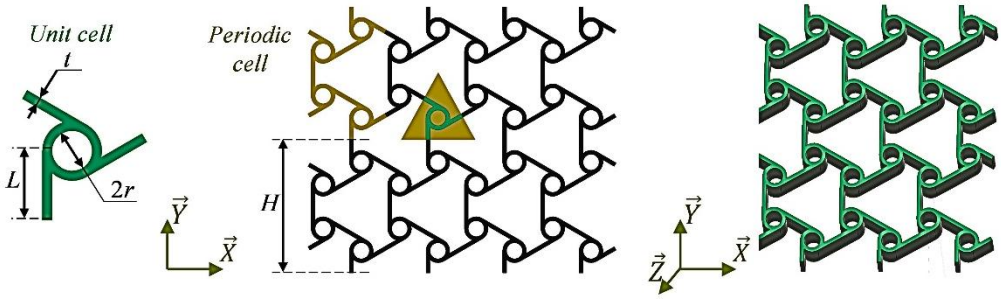


Figure 2. Antitrichiral lattice.

$$\frac{\rho}{\rho_s} = \frac{2\sqrt{3}\,t}{H^2}\left(\pi r + \frac{3}{2}L\right) \tag{1}$$

$$L = \frac{H}{6} \tag{2}$$

Table I Geometric parameters used for the antitrichiral lattice.

L (mm)	Test reference	$r(mm)$	*ρ/ρs (%)*	*H (mm)*	*b (mm)*	*t (mm)*	*e (mm)*
4.16 (1 CW)	ST1	0.0	8.30	25	25	0.6	5
	ST2	0.4	9.97				
	ST3	0.8	11.64				
	ST4	2.2	17.48				
	ST5	3.2	21.65				
2.08 (2 CW)	ST6	0.0	16.65	25/2	25	0.6	5
	ST7	0.4	23.36				
	ST8	0.8	30.06				
	ST9	1.2	36.76				
1.38 (3 CW)	ST10	0.4	39,93	25/3	25	0.6	5

2.3 Experimental Protocols

To characterize the mechanical behavior of the sandwich structures with architected cores described in Section 2.2, compression tests were first conducted to evaluate their load-bearing capacity and deformation response under axial loading. In addition, indentation tests were performed to provide a comprehensive assessment of the static mechanical performance of the sandwich panels. These experiments are essential for evaluating and comparing the energy absorption capability of the anti-trichiral lattice, offering valuable insights into the influence of geometric parameters on overall structural performance and their potential relevance for specific engineering applications.

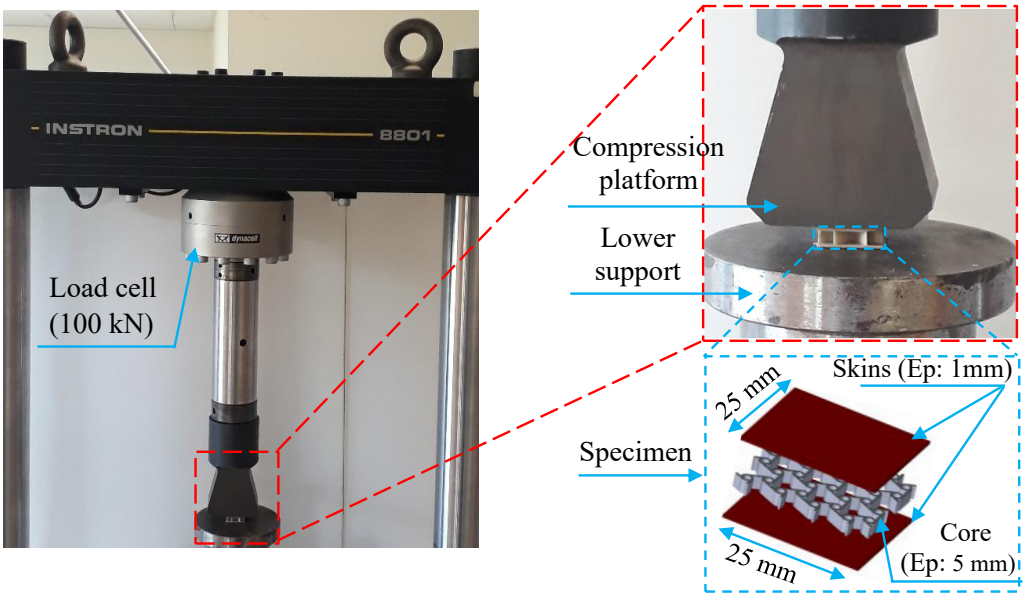


Figure 3. Experimental compression system.

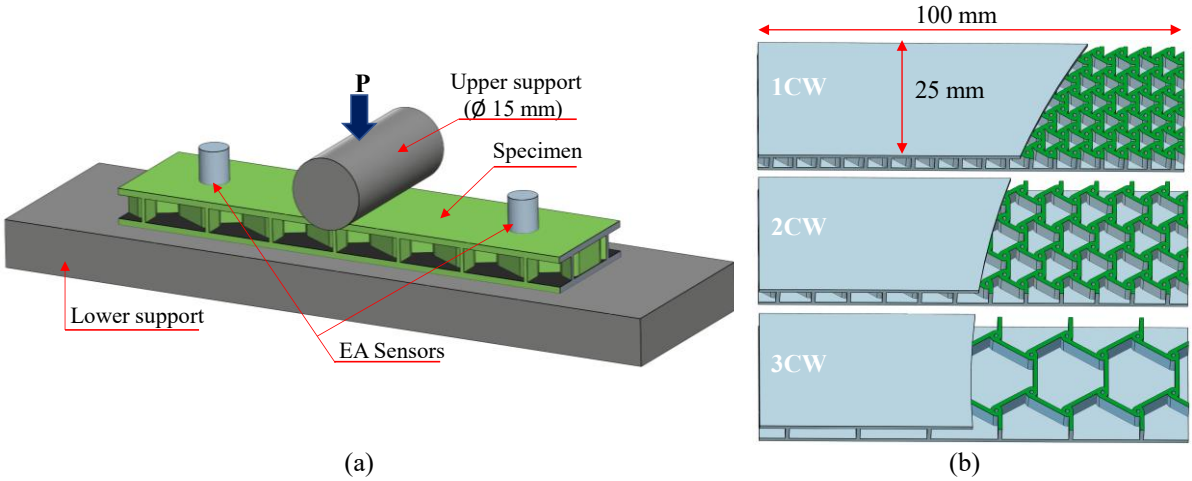


Figure 4. (a) Experimental indentation system and (b) Indentation specimens.

To assess the stiffness, strength, and energy absorption capacity of the structured cores, sandwich panels with the geometries and parameters defined in Section 2.2 were subjected to compression testing. The experimental setup, illustrated in Figure 3, includes a universal testing machine equipped with a 100 kN load cell operating in accordance with the ASTM C365 standard [54]. The compressive load was applied through two rigid parallel plates. The test specimens were 3D printed with overall dimensions of 25 × 25 × 7 mm, as shown in Figure 3.
To investigate the mechanical behavior and energy absorption capacity of sandwich materials, quasi-static indentation tests were performed. These experiments allow for a detailed evaluation of how geometric and material

parameters, such as node radius, ligament length, and core density, affect the mechanical response and energy absorption characteristics of the sandwich panels. The testing procedure was carried out using a universal testing machine equipped with a 10 kN load cell, as presented in Figure 4(a). During testing, a load P was applied by a cylindrical indenter centered on the sandwich specimen, which was supported on a rigid platform and loaded at a constant displacement rate of 1 mm/min. The specimens were 3D printed with dimensions of 100 × 25 × 7 mm, as illustrated in Figure 4(b), and incorporated different core configurations listed in Table I.

3. Experimental Results and Interpretation

3.1 Compression response of sandwich panels

Mechanical characterization of architected core sandwich panels is essential because their global stiffness, strength, and energy absorption capacity are governed by the periodic core geometry rather than by bulk material properties alone. Through thickness compression tests are particularly informative, since they activate the dominant deformation mechanisms of the lattice (bending and buckling of ligaments) and reveal how geometric parameters such as node radius and core thickness affect load transfer between the facesheets. These tests also quantify the compression modulus and the dissipated energy, which are key design metrics for lightweight structures used in impact mitigation and transportation applications.

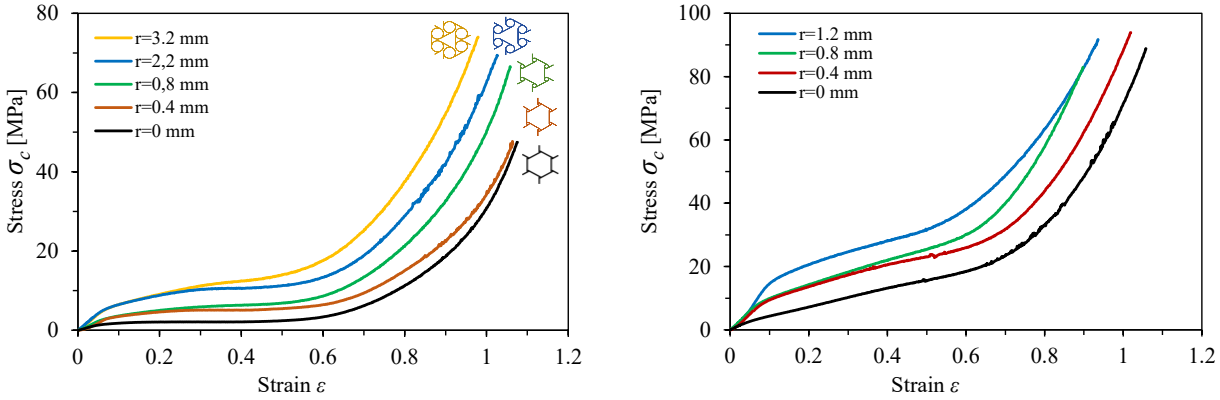


Figure 5. Compressive properties of antitrichiral sandwiches with varying node radii: (a) single-cell-wide (1CW) configurations and (b) two-cell-wide (2CW) configurations.

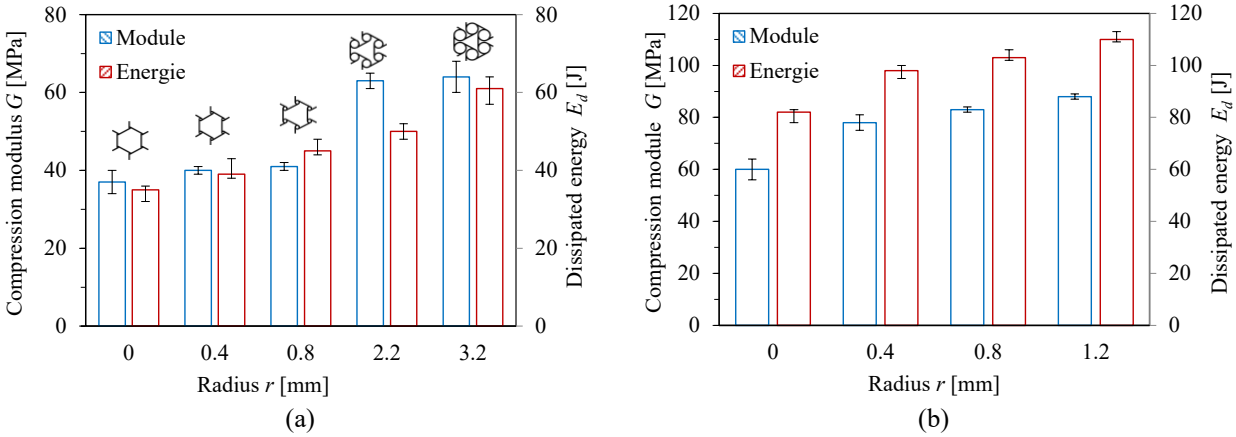
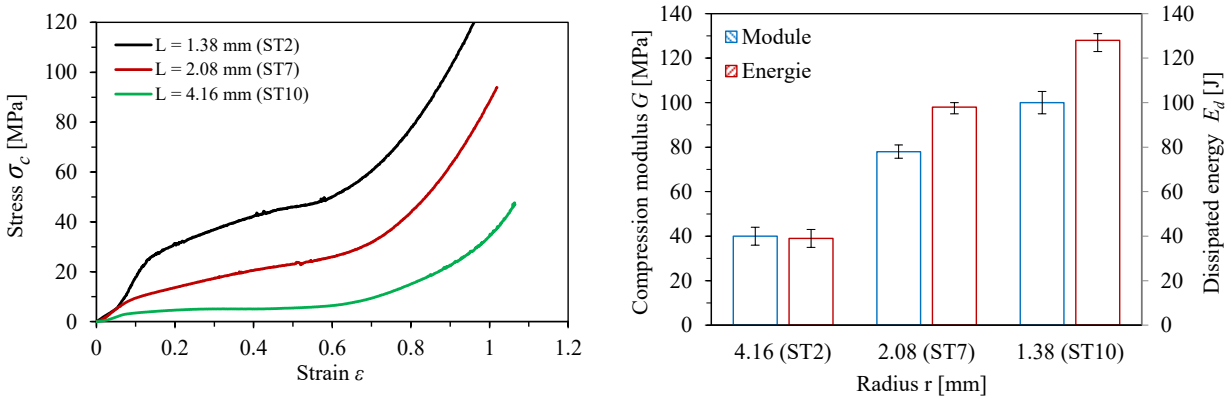


Figure 6. Compression modulus and dissipated energy of antitrichiral sandwiches with varying node radii: (a) single-cell-wide (1CW) configurations and (b) two-cell-wide (2CW) configurations.

For Figure 5(a), the single cell wide (1CW) sandwiches with L=4.16 mm exhibit a nonlinear stress–strain response that evolves markedly with node radius r. The reference specimen ST1, with r=0 and the lowest relative density $\rho/\rho s$=8.30, shows the most compliant behavior: the initial slope of the curve is modest and the stress increases gradually with strain up to $\varepsilon \approx 1$, indicating a deformation regime dominated by buckling of relatively slender ligaments. As r increases to 0.4 mm (ST2) and 0.8 mm (ST3), the curves shift upward and become steeper, reflecting a higher compression modulus and higher stresses at any given strain due to thicker nodes, shorter

effective ligament spans, and a partial shift from bending dominated to more stretch dominated load transfer. The largest radii, 2.2 mm (ST4) and 3.2 mm (ST5), lead to the stiffest response: stresses rise rapidly beyond $\varepsilon \approx 0.4$ and reach the highest values before failure and indicating that the cell topology with large nodes stabilizes the ligaments against premature buckling. Overall, Figure 5(a) demonstrates that, in 1CW configurations, increasing node radius monotonically increases stiffness and load bearing capacity but simultaneously increases relative density, highlighting a tradeoff between lightweight design and mechanical performance typical of antitrichiral lattices.



(a) (b)

Figure 7. Compressive properties of antitrichiral structures with fixed node radius r=0.4 mm and varying ligament lengths: (a) stress-strain curves and (b) compressive modulus and dissipated energy.

Figure 5(b) presents the stress-strain curves for the two cell wide (2CW) sandwiches with L=2.08 mm, where the cell number is doubled with respect to the 1CW case. Even for the baseline specimen ST6 with r=0, the curve lies significantly above that of ST1, indicating that increasing the number of cells through the thickness enhances global stiffness and strength by engaging more ligaments in load sharing and improving confinement between facesheets. As the node radius grows from 0.4 mm (ST7) to 0.8 mm (ST8) and 1.2 mm (ST9), the stress-strain curves exhibit a systematic upward shift similar to the 1CW case but at consistently higher stress levels, with the ST9 curve showing the highest stresses up to strains around 0.9-1.0. When configurations with the same radius are compared between Figures 5(a) and 5(b) (for r=0,0.4,0.8 mm), the 2CW cores always sustain higher stresses over the full strain range, revealing that increasing cell number is a very effective strategy for enhancing compressive performance, especially when combined with larger node radii that promote stretch dominated behavior and delay instability.

Figure 6(a) summarizes for the 1CW sandwiches the evolution of compression modulus G and dissipated energy E_d as functions of node radius. The results show that G increases monotonically from the lowest value for ST1to the highest values for ST4 and ST5, approximately doubling as the relative density increases by a factor of about 2.5. The dissipated energy follows the same trend but with a slightly stronger sensitivity to r: specimens with larger nodes not only have higher modulus but also maintain higher stress levels over the whole strain range, leading to a larger area under the curve and therefore greater energy absorption up to the prescribed maximum strain. Comparing ST1 and ST5, the increase in node radius and relative density yields a substantial improvement in both stiffness and dissipated energy, suggesting that within the explored range the specific energy absorption (energy per unit mass) can still improve despite the higher density, which is attractive for crashworthy yet lightweight designs.

Figure 6(b) provides the corresponding modulus and energy metrics for the 2CW sandwiches and highlights the benefits of increasing core thickness in combination with node radius. The compression modulus values for ST6-ST9 are significantly higher than for ST1-ST5 at comparable radii: for example, at r=0.8 mm (ST3 vs. ST8), the 2CW configuration achieves a much larger G while the relative density increases from 11.64 to 30.06, showing that the stiffness gain outpaces the added mass when moving to a denser core. The dissipated energy bars in Figure 6(b) also rise steeply with radius, with ST9 displaying the highest E_d, which reflects the high stress levels and extended deformation before densification observed in Figure 5(b). When 1CW and 2CW data are compared at the same radii r=0,0.4,0.8 mm, the 2CW sandwiches exhibit systematically higher G and E_d than their 1CW counterparts, indicating that combining a multi cell thick antitrichiral core with increased node radius is an efficient route to achieving superior stiffness and energy absorption performance for sandwich structures subject to compressive loading.

For the antitrichiral structures in Figure 7, keeping the node radius fixed at r=0.4 mm while reducing the ligament length L from 4.16 mm (ST2, one cell wide: 1CW) to 2.08 mm (ST7, two cells wide: 2CW) and then to 1.38 mm (ST10, three cells wide: 3CW) significantly increases compressive stiffness, strength, and energy absorption. The stress-strain curves for ST2, ST7, and ST10 show a clear and systematic upward shift as L decreases, i.e. as the ligament core becomes long in terms of cell count. ST2 exhibits the most compliant response: after a modest initial slope, the stress rises slowly with strain, reaching the lowest stress level at $\varepsilon \approx 1.0$. The curve for ST7 lies distinctly above ST2 over the entire strain range: the initial slope is higher and the stress at moderate strains ($\varepsilon \approx$ 0.4-0.6) is roughly two times that of ST2, showing that adding cell in the specimen stiffens the structure and delays the onset of strong nonlinearity. ST10 shows the stiffest response, with the highest initial slope and a very steep stress increase beyond $\varepsilon \approx 0.4$; the curve reaches peak stresses well above those of ST7 and ST2 at comparable strains.

Figure 7(b) quantifies these observations by presenting the compression modulus G and dissipated energy E_d for ST2, ST7, and ST10. The modulus bars show a nearly monotonic increase as L decreases: ST2 has the lowest G, ST7 exhibits an intermediate value, and ST10 reaches the highest modulus, roughly a factor of two-three larger than that of ST2. The dissipated energy E_d follows the same trend but with an even more pronounced increase: the results indicate that ST7 stores and dissipates significantly more energy than ST2, while ST10 shows the largest E_d, on the order of 1.5-2 times that of ST7 and several times that of ST2, reflecting the much larger area under its stress-strain curve up to the target strain.

From a mechanical design perspective, the comparison of ST2, ST7, and ST10 underscores that, at fixed local geometry (same node radius), tailoring ligament length is an effective strategy to tune the global response of antitrichiral sandwiches. Shorter ligaments and more cells simultaneously increase stiffness and enhance energy absorption, because they (i) reduce bending lengths, (ii) introduce more load paths in series and parallel, and (iii) delay localized buckling, leading to a more stable, gradually hardening compressive response desirable for protective, crashworthy, or vibration mitigating applications.

3.2 Indentation response of sandwich panels

Indentation testing provides a direct way to characterize the local stiffness, strength, and energy-absorption capacity of sandwich panels with antitrichiral cores. By applying a concentrated load through a cylindrical indenter and recording the load-displacement response, it is possible to quantify how geometric parameters such as node radius r, ligament length L, and the number of cells across the width (1CW, 2CW, 3CW) influence the resistance to localized damage, which is critical for contact-loading applications.

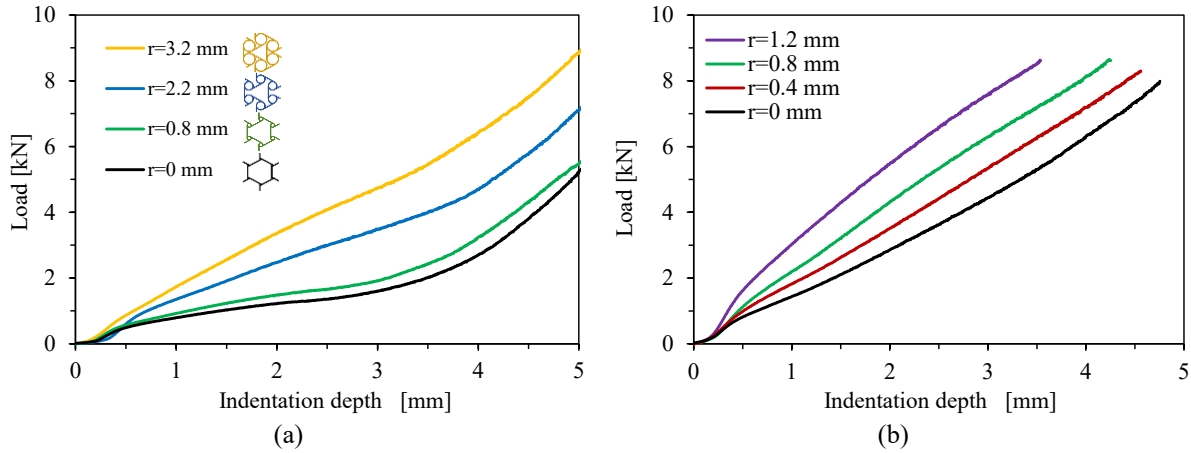


Figure 8. Load-indentation depth of antitrichiral structures with varying node radii: (a) single-cell-wide (1CW) configurations and (b) two-cell-wide (2CW) configurations.

The load-indentation curves in Figures 8 show that increasing the node radius r (and thus the relative density $\rho/\rho s$) systematically increases the indentation stiffness and load-carrying capacity of the antitrichiral cores over the whole depth range up to 5 mm. For the 1-cell-wide (1CW, L=4.16 mm) specimens, the load-indentation curves show a clear increase in stiffness and load-carrying capacity with increasing node radius and relative density. ST1 gives the softest response, reaching about 5 kN at 5 mm. ST3 lies above ST1. ST4 shows a higher slope and reaches about 7 kN, while ST5 is the stiffest, attaining around 9 kN. Thus, for 1CW cores, the load at a given indentation

depth increases monotonically with r. For the 2-cell-wide (2CW, L=2.08 mm) specimens, the same trend appears, but at overall higher loads due to the greater number of cells across the width and higher relative densities. ST6 is the most compliant. ST7, ST8, and ST9 show progressively higher slopes. The curves are smooth and nearly linear beyond approximately 0.5 mm, indicating stable progressive deformation without abrupt failure.

Figure 9 presents the dissipated energy as a function of indentation depth. All curves are monotonically increasing and convex, showing that the incremental energy absorbed per unit displacement rises as indentation progresses. For 1CW specimens, the hierarchy of curves mirrors Figure 9: ST5 (r=3.2 mm) dissipates the most energy, reaching about 20 J at 5 mm, followed by ST4 (15 J), ST3 (10 J), and ST1 (8J). Thus, increasing r more than doubles the energy absorbed between the most open (ST1) and the densest (ST5) core. For 2CW specimens, the same monotonic trend is observed. At any indentation depth, larger node radii and higher relative densities yield greater energy absorption.

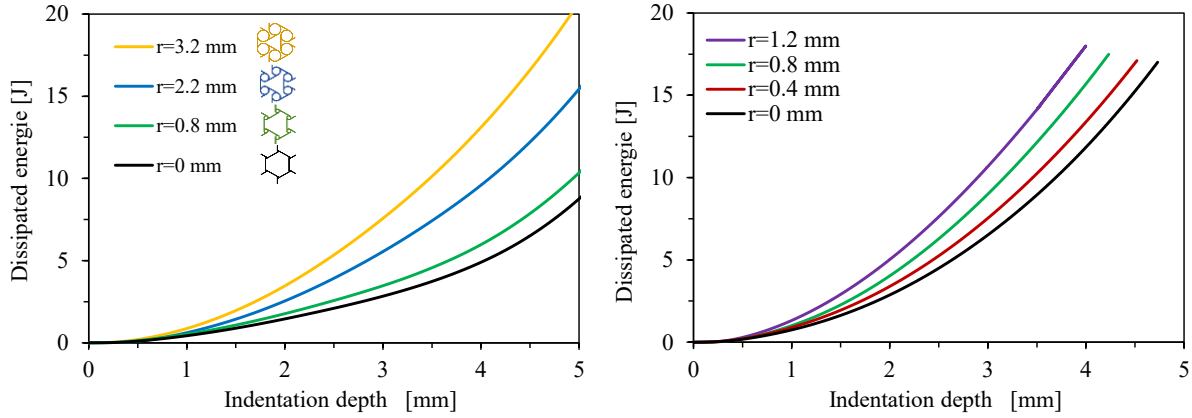


Figure 9. Dissipated energy- indentation depth of antitrichiral structures with varying node radii: (a) single-cell-wide (1CW) configurations and (b) two-cell-wide (2CW) configurations.

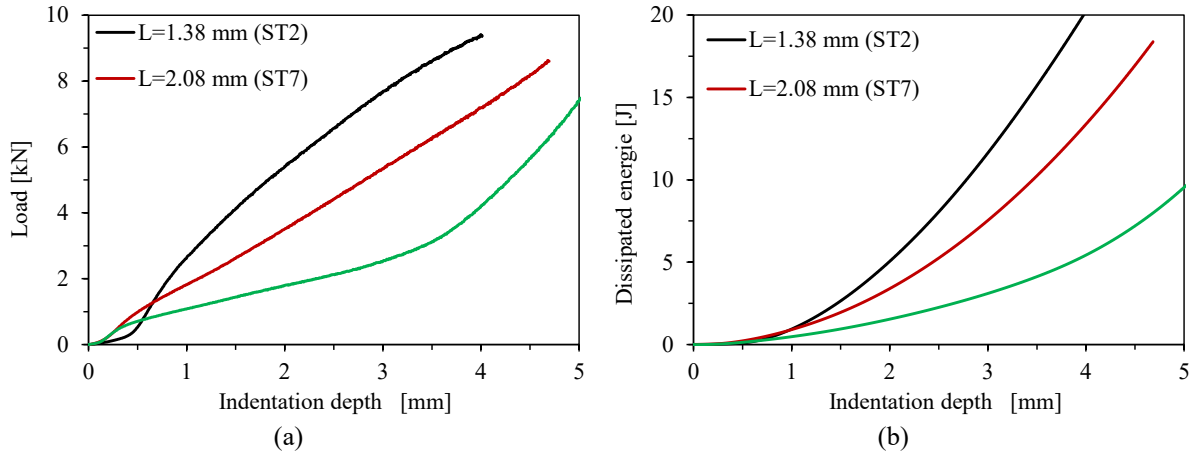


Figure 10. Indentation properties of antitrichiral structures with fixed node radius r=0.4 mm and varying ligament lengths: (a) Load-indentation depth and (b) dissipated energy- indentation depth.

Figure 10 compares three specimens with identical node radius (r=0.4 mm) but different ligament lengths. In Fig. 10(a), the load-indentation curves show that decreasing L (and increasing the number of cells across the width) significantly increases stiffness and load capacity. The shortest ligament, 3CW specimen ST10 exhibits the steepest response, reaching around 9.5 kN at 4 mm. The 2CW specimen ST7 is intermediate, attaining about 7.5 kN, while the longest ligament 1CW specimen ST2 is the most compliant and reaches the lowest load at a given indentation depth. In Fig. 10(b), the dissipated energy curves reflect the same ranking. At 4 mm indentation, ST10 absorbs the most energy (20 J), ST7 is intermediate (about 13 J), and ST2 absorbs the least (5 J). Again, all curves are convex, with more rapid energy accumulation at larger depths for the stiffer, denser structures.

Across all figures, the results show a consistent, physically intuitive behavior:

- At fixed ligament length (1CW or 2CW), increasing node radius r and relative density increases indentation stiffness, peak load, and dissipated energy (ST1 → ST3 → ST4 → ST5 for 1CW; ST6 → ST7 → ST8 → ST9 for 2CW).
- At fixed node radius (r=0.4 mm), decreasing ligament length L and increasing the number of cells across the width (1CW → 2CW → 3CW) also increases stiffness, load capacity, and energy absorption.

Mechanically, larger nodes and shorter ligaments both enhance the bending and stretching stiffness of the antitrichiral lattice. Increasing r thickens the load paths, shifting the response toward a more stretch-dominated regime with higher effective modulus and strength. Reducing L shortens the lever arms of the ligaments, making them harder to bend and increasing the number of load-bearing members per unit area. Both effects raise the effective relative density, so more material participates in carrying load and storing (and then dissipating) deformation energy.

The comparison between 1CW and 2CW at similar r (e.g., ST3 vs. ST8, both with r=0.8 mm) and between 2CW and 3CW at fixed r=0.4 mm (ST7 vs. ST10) shows that increasing the number of cells across the width can be as influential as increasing node radius: wider cells count distribute the contact load over multiple ligaments, delay local crushing, and significantly enhance both load capacity and energy absorption. This design flexibility is characteristic of auxetic and antichiral lattices and is highly advantageous for tailoring sandwich cores to specific indentation and impact resistance requirements.

Together, the results demonstrate that antitrichiral cores provide tunable indentation performance: by appropriately choosing node radius and ligament length (and thus relative density and cell count), one can trade off weight against stiffness and energy absorption. For applications where high localized impact resistance is needed, dense configurations with large node radii and short ligaments (such as ST9 or ST10) are preferable, whereas more open geometries (e.g., ST1 or ST2) may be chosen when weight reduction is prioritized over maximum indentation resistance.

4. Conclusion

The experimental investigation on 3D-printed PLA/flax sandwich panels with anti-trichiral cores demonstrates that geometric tailoring of the lattice provides a powerful and reliable means to tune stiffness and energy absorption while maintaining low weight and sustainable material content. At a global level, the results confirm that anti-trichiral cores exhibit the characteristic advantages of auxetic architecturesstable plateau response, progressive collapse, and high deformation capacity when subjected to both through-thickness compression and localized indentation. By systematically varying node radius, ligament length, and the number of cells across the width, the study quantifies how relatively simple geometric changes translate into significant performance gains under quasi-static loading.

From a quantitative standpoint, increasing the node radius from the most open to the densest configuration led to marked improvements in mechanical performance. For the single-cell-wide (1CW) cores, the compression modulus and the dissipated energy up to failure increased by roughly 75% between the smallest and largest node radii. A similar trend was observed in indentation, where the maximum load at a fixed penetration depth increased by approximately 60-120%, and the area under the load-displacement curve (a proxy for indentation energy absorption) rose by about 100-200% as node radius and relative density increased. These results underline that node thickening, though it raises density, offers a highly effective lever to boost both stiffness and energy absorption in anti-trichiral lattices.

The influence of ligament length and cell count was equally significant. At fixed node radius, reducing ligament length and increasing the number of cells across the width from 1CW to 3CW yielded increases in compression modulus of approximately 100-150%, depending on the configuration, while the dissipated energy grew by roughly 150-225% over the same range of geometrical refinement. In indentation, the shortest-ligament, three-cell-wide cores carried loads up to around 100-200% higher at a given indentation depth, and absorbed roughly two to four times more energy compared with the longest-ligament, single-cell-wide specimens. These comparative results show that shortening ligaments and stacking more cells is as influential as increasing node radius, providing complementary design strategies: one can increase stiffness and energy absorption either by thickening nodes, by refining the lattice in the transverse direction, or by combining both approaches, depending on mass and manufacturability constraints.

When viewed against typical non-auxetic or conventional lattice cores reported in the literature, the anti-trichiral PLA/flax structures developed in this work exhibit competitive or superior specific energy absorption, while also benefiting from auxetic deformation modes that delay localization and sudden collapse. The use of a PLA/flax biocomposite further enhances the attractiveness of the concept, since the natural-fiber reinforcement improves stiffness and strength compared with neat PLA, and the material system is bio-based and potentially biodegradable,

aligning the mechanical design with sustainability requirements. In this sense, the work demonstrates that architected bio-based metamaterials can meet both mechanical and environmental objectives, reducing reliance on petroleum-based or metallic systems for certain impact-mitigation and lightweight structural applications.
Overall, the study provides a clear geometry-performance map for anti-trichiral PLA/flax cores, showing that variations in node radius and ligament length can lead to gains of 75-150% in stiffness and 100-225% in dissipated energy, depending on the chosen metric and loading mode. These quantitative trends offer practical guidance for designing sandwich panels where compression and indentation resistance are critical, without changing the material system or production process. Future work should extend the present quasi-static characterization to dynamic and fatigue loading, and integrate numerical optimization and multi-objective design frameworks to explore the broader design space of anti-trichiral cores, including graded architectures and hybrid materials, with the goal of further improving performance while preserving or enhancing sustainability.

Data availability The proposed research does not use any datasets.

Statements and Declarations: The authors have no relevant financial or non-financial interests to disclose.
.

References

1. V. Tuninetti, S. Narayan, I. Ríos, B. Menacer, R. Valle, M. Al-Lehaibi, M. U. Kaisan, J. Samuel, A. Oñate, and G. Pincheira, Biomimetics **10**, 458 (2025).
2. P. Qiao, M. Yang, and F. Bobaru, J. Aerosp. Eng. **21**, 235 (2008).
3. D. F. Braga, S. M. O. Tavares, L. F. Da Silva, P. Moreira, and P. M. De Castro, Progress in Aerospace Sciences **69**, 29 (2014).
4. Q. H. Alsultan, A. S. Abdulbaqi, S. M. Nejrs, S. A. Jassim, B. H. Sulaiman, O. S. Al deen Shawqi, T. H. Abed, I. Y. Panessai, and H. A. Khalaf, Khwarizmia **2023**, 63 (2023).
5. D. M. Frangopol and K. Maute, Computers & Structures **81**, 397 (2003).
6. L. Torre and J. M. Kenny, Composite Structures **50**, 257 (2000).
7. L. A. Twisdale, R. H. Sues, and F. M. Lavelle, Structural Safety **15**, 17 (1994).
8. S. Yin, H. Chen, J. Li, T. X. Yu, and J. Xu, International Journal of Mechanical Sciences **157**, 282 (2019).
9. C. Dapogny, A. Faure, G. Michailidis, G. Allaire, A. Couvelas, and R. Estevez, Computational Mechanics **59**, 933 (2017).
10. A. Hamrouni, J.-L. Rebiere, A. El Mahi, M. Beyaoui, and M. Haddar, Jnl of Sandwich Structures & Materials **25**, 426 (2023).
11. T. Li, F. Liu, and L. Wang, Composites Part B: Engineering **198**, 108229 (2020).
12. P. U. Kelkar, H. S. Kim, K.-H. Cho, J. Y. Kwak, C.-Y. Kang, and H.-C. Song, Sensors **20**, 3132 (2020).
13. M. Mohammadpour and F. Taheri-Behrooz, Jnl of Sandwich Structures & Materials **26**, 1165 (2024).
14. A. Hamrouni, J.-L. Rebiere, A. E. Mahi, M. Beyaoui, and M. Haddar, Int J Interact Des Manuf (2025).
15. A. Hamrouni, J.-L. Rebiere, A. El Mahi, M. Beyaoui, and M. Haddar, Journal of Vibration and Control 10775463231185914 (2023).
16. G. Wang, S. Wan, J. Hong, L. Li, S. Liu, and X. Li, Engineering Structures **315**, 118502 (2024).
17. X. Chen, S. Zhuang, T. He, and M. Feng, Mechanics of Advanced Materials and Structures **32**, 3423 (2025).
18. A. Hamrouni, J.-L. Rebiere, A. El Mahi, M. Beyaoui, and M. Haddar, Journal of Composite Materials **57**, 2161 (2023).
19. A. Gupta, S. Sharma, R. R. Madke, and R. Chowdhury, International Journal of Mechanical Sciences **289**, 110054 (2025).
20. D. Mousanezhad, B. Haghpanah, R. Ghosh, A. M. Hamouda, H. Nayeb-Hashemi, and A. Vaziri, Theoretical and Applied Mechanics Letters **6**, 81 (2016).
21. Q. Shao, C. Ding, X. Ji, J. Mu, X. Wang, and Y. Xue, Journal of Materials Research and Technology **32**, 841 (2024).
22. C. Raef, M. Abid, M. Amine Ben Souf, and S. Ahmed, in *INTER-NOISE and NOISE-CON Congress and Conference Proceedings* (Institute of Noise Control Engineering, 2025), pp. 2761–2769.
23. R. Siakeng, M. Jawaid, H. Ariffin, S. M. Sapuan, M. Asim, and N. Saba, Polymer Composites **40**, 446 (2019).
24. O. Faruk, A. K. Bledzki, H.-P. Fink, and M. Sain, Progress in Polymer Science **37**, 1552 (2012).
25. T. D. Ngo, M. Nofar, M. T. Ton-That, and W. Hu, Journal of Composite Materials **50**, 3043 (2016).

26. M. N. Ahmad, M. R. Ishak, and M. Z. Z. Hannah, J. Adv. Res. Appl. Mech **123**, 238 (2024).
27. S. Charca, L. Jiao-Wang, and C. Santiuste, Materials **17**, 2958 (2024).
28. D. Lascano, R. Guillen-Pineda, L. Quiles-Carrillo, J. Ivorra-Martínez, R. Balart, N. Montanes, and T. Boronat, Polymers **13**, 342 (2021).
29. D. Wannarong and T. Singhanart, Engineering Journal **26**, 27 (2022).
30. A. Hamrouni, J.-L. Rebiere, A. El Mahi, M. Beyaoui, and M. Haddar, Int. J. Appl. Mechanics **14**, 2250025 (2022).
31. B. Bax and J. Müssig, Composites Science and Technology **68**, 1601 (2008).
32. (n.d.).
33. C. Chen, W. Xu, H. Hai, Z. Zhao, W. Sun, W. Wang, and S. Cheng, Int J Mech Mater Des **21**, 627 (2025).